1116

NRL Memorandum Report 1116

HYPERVELOCITY PROJECTION TECHNIQUES AND IMPACT STUDIES JANUARY 1959 - JUNE 1960

W. W. Atkins
S. M. Halperson

MECHANICS DIVISION

November 1960

U. S. NAVAL RESEARCH LABORATORY
Washington, D.C.

NRL MEMORANDUM REPORT

NO. 1116

HYPERVELOCITY PROJECTION TECHNIQUES AND IMPACT STUDIES JANUARY 1959 - JUNE 1960

W. W. Atkins
S. M. Halperson

Mechanics Division

November 1960

U. S. NAVAL RESEARCH LABORATORY
Washington, D. C.

CONTENTS

ABSTRACT

The Bureau of Naval Weapons has initiated a program at the U.S. Naval Research Laboratory to obtain terminal ballistic data for masses up to five grams starting at velocities of 4.6 km/sec and extending into the hypervelocity region as far as possible. Evacuated-range facilities and special high-velocity accelerators were constructed for this purpose. The expendable-breech light-gas gun developed at NRL was the primary accelerator. Instrumentation such as an accurate velocity-measuring system was developed to cope with the special problems inherent in high-velocity work. A large amount of terminal ballistic data has been obtained using aluminum and tungsten carbide projectiles at velocities from near zero to 6.4 km/sec. Both conventional powder guns and light-gas guns were used to obtain this data. Various target materials were examined including lead, steel, copper and two kinds of aluminum, 1100 F and 2014-T6. Much valuable information about hypervelocity impact was obtained from these tests. The data show that for the velocity range and materials considered, the cavity shape approaches that of a hemisphere when the impact is in the hypervelocity region. Also, the ratio of impact energy to crater volume as a function of impact velocity seems to approach a constant value in the hypervelocity region for each projectile-target system except for tungsten carbide into lead.

PROBLEM STATUS

This is the final report for NRL Problem 62F04-07. Work on the problem will continue under NRL Problem 62F04-04.

AUTHORIZATION

NRL Problem 62F04-07
Project No. NO-508-925/53024/02-135

NRL Problem 62F04-04
Project No. NR 503 00c

Hypervelocity Projection Techniques and Impact Studies
January 1959 - June 1960

INTRODUCTION

A Bureau of Naval Weapons sponsored project was initiated at the U.S. Naval Research Laboratory in September 1956 to develop ballistic facilities capable of firing projectiles weighing up to five grams to 4.6 km/sec and above. This equipment was to be used for basic terminal ballistic studies extending to velocities as high as possible. The third model of the expendable-breech light-gas gun developed at NRL (1) more than meets the ballistic requirements of the project.

In order to obtain ballistic data at the required velocities, firings must be made in a controlled, reduced-pressure atmosphere; therefore suitable ranges were designed and constructed. At present two ranges are available for use, and a third will be completed shortly. These ranges can be evacuated to pressures equivalent to those reached at altitudes up to 180,000 feet.

During initial range tests, existing velocity-measurement and photographic techniques proved inadequate for hypervelocity vacuum firings, so an instrumentation-development program was begun. A highly dependable velocity-measuring system has been developed that is capable of extremely high accuracies.

The completed ballistic-range facilities have been in operation for some time, and much terminal ballistic data have been gathered.

To date, the studies have attempted to determine the mechanisms involved in hypervelocity impact damage. Thick metallic targets were investigated. Target materials included lead, copper, steel, 1100 F, and 2014 aluminum. Projectiles were either tungsten carbide or 2014 aluminum with a velocity range from near zero to 6.4 km/sec. The characteristics of target cratering investigated include cavity shape and depth of penetration as a function of impact velocity and the relationships between crater volume and energy of the impinging projectile.

FACILITIES AND INSTRUMENTATION

The two completed hypervelocity ranges now in operation have been described in detail in previous reports (2). Each consists of an expendable-breech-gas gun, a sealed system extending from the launch tube to the target that can be evacuated to 0.5 mm Hg, (Fig. 1), and a photographic velocity-measuring unit capable of determining projectile velocity, orientation, and general condition.

Basic models of the two-stage expendable-breech light-gas gun have successfully fired projectiles weighing from 0.1 to 140 grams and have achieved maximum velocities above 5.8 km/sec.* The firing

*Since the period covered in this report, a light-gas gun at this facility has reached velocities exceeding 7.3 km/sec.

cycle of one of these guns begins with the injection of a low-molecular-weight gas into a gun barrel sealed at both ends and then adiabatically compressing the gas with a gunpowder-driven piston to temperatures and pressures well above those attained in conventional powder gas. This high-pressure, high-temperature gas is then allowed to expand down a smaller diameter gun barrel, propelling a projectile ahead of it. Because of its low molecular weight and high temperature, the free-flow velocity of the gas is considerably higher than that of the accelerating gas in a powder gun, and therefore the maximum attainable projectile velocity is substantially higher than the 3 km/sec limit of powder guns.

The velocity-measuring technique that has proven most effective for hypervelocity firings utilizes a high-speed motion-picture camera, a high-frequency time-mark generator, two or more continuous light sources and associated optical slits, and a complex of lenses and mirrors. The slits are mounted perpendicularly to the trajectory and are illuminated by the light sources so that a passing projectile will place a sharp shadow on them. The light passing through the slits is focused into the camera so that each slit wipes a continuous stripe on the fast-moving film. As the projectile progresses across a slit, part of the slit's light is interrupted, which in turn interrupts the stripe being wiped onto the film. Shadow images of the projectile are placed onto the moving film as the projectile passes each slit.

The high-frequency time-mark generator places marks on the film at a predetermined frequency; this allows the film velocity to be computed. The image displacement along the film together with known film velocity and slit spacing are sufficient to determine projectile velocity. By careful examination of these images, projectile orientation and condition can also be determined. Figure 2 shows a diagram of a single velocity measuring station.

GUN DEVELOPMENT

Although the present capability of the light-gas gun represents a substantial improvement over previous ballistic accelerators, still higher velocities are required for the effective study of meteoric impacts and AICBM defense systems. Of immediate interest are data in the velocity range between 6 and 15 km/sec. In order to attain such capabilities, a development program has been initiated to improve the gas gun's performance. Thus far the highest velocities for a relatively high mass have been achieved with a three-stage light-gas gun (3). A theoretical study of the dynamics of the light-gas has begun (4), and it is expected that this study will prove useful in optimization of gun parameters.

The three-stage gun (Fig. 3) consists of a 37-mm pump section using a two-pound standard piston. The gas compressed in the 37-mm barrel is used to drive a second piston down a 20-mm barrel to velocities

well above those attained in normal gunpowder firings. The gas compressed by the high-speed 20-mm piston then accelerates a small projectile down a 35-cal launch tube. Using this technique, a 1.3-gram projectile has been accelerated to a maximum velocity of 6.4 km/sec. A two-stage gun consisting of a 20-mm pump tube and a 30-cal launch tube, utilizing the same powder load and gas pressure as the three-stage gun, attained velocities of 5.5 km/sec. The higher velocity of the three-stage gun can be attributed to its greater 20-mm piston velocity.

HYPERVELOCITY PENETRATION STUDIES

A large amount of terminal ballistic information has been obtained from successful light-gas-gun firings. Thick targets of lead, copper, steel, 1100 F, and 2014 aluminum were examined. Various characteristics of target cratering will be discussed in detail below. Work with spaced structure targets has also begun, but is only in its beginning phases.

Target Cratering

Characteristic Shape - Figure 4 is a graph which illustrates the change in cavity shape as a function of impact velocity. The ordinate is the ratio of the depth of penetration P to the crater diameter D_c as measured across the original surface of the target. When this ratio is large, a tunnel-shaped crater is indicated. As the curves approach the 0.5 value for P/D_c, the shape of the cavity approaches that of a hemisphere. Tungsten carbide or 2014 aluminum projectiles having

various masses were employed in this study. The projectiles were either spheres or cylinders. Since cratering of the steel targets struck by tungsten carbide is very pronounced, the diameters of these craters measured across the original surfaces are noticeably smaller than they are half way into the crater. This illustrates the fact that the cavity shape is still to a significant extent dependent upon target-material strength. One criterion for the onset of hypervelocity impact is that the cavity shape must be approximately that of a hemisphere. From the figures it is evident that no single numerical value can be assigned for the beginning of this velocity region. This value is a function of both the target and projectile materials.

The curves in Fig. 5 illustrate the effect of the strength of the projectile-target system, and also the fact that the impact is far from being in the hypervelocity region. It is evident from the figure that additional data points are necessary to define these curves; however, their general shapes are indicated. The maxima of these curves as well as those shown in Fig. 4 are determined primarily by the behavior of the penetrator and occur due to projectile shattering. Since the deformation of the aluminum projectile is gradual as opposed to the rather abrupt shattering of the tungsten carbide sphere, no peaks are observed in the aluminum-projectile data.

Figure 6 is a front and sectional view of two craters in 1100 F Al produced by aluminum projectiles having an impact velocity of 6.4 km/sec. The black rectangle represents the projectile size (before

firing) relative to that of the cavity. The in-gun weight and diameter of the projectile were 1.27 g and 0.35 in. Based on the results shown in Figs. 9 and 12, to be discussed later, the actual mass striking the target was estimated to be 0.7 g, and the projectile had a diameter of approximately 0.26 in. The smaller crater was formed by impact of a fragment from the projectile shear disc. By assuming a constant energy per unit volume (Fig. 12), this small fragment would have a mass of 0.122 milligrams and, if spherical, a diameter of 0.44 mm.

Another feature of hypervelocity projectile impact into thick targets is the similarity of crater shape independent of projectile mass. This is shown by the cavities of Fig. 6. The characteristic crater shape, in the hypervelocity region, is also shown by Fig. 4 to be independent of the material properties of the projectile-target system.

Penetration - Turning now from considerations of cavity shape, Fig. 7 is a graph of target penetration P divided by projectile diameter D_s as a function of impact velocity. Indicated with each curve is the projectile-target combination. All projectiles were spherical, saboted during acceleration, and appeared to have no reduction of mass in transit. Impact masses of the projectiles were 1.27 g for the 0.375-in.-dia Al sphere, 2.00 g for the 0.25-in.-dia WC sphere, and 0.25 g for the 0.125-in.-dia WC sphere. The effect of sphere shattering in the low-velocity region is again clearly evident, and this shattering results in an actual decrease in penetration. Because of

the broad peak in the P/D_c curve (Fig. 4), the data of Fig. 7 in the 1 km/sec region are insufficient to indicate a corresponding peak.

Figure 8 is similar to Fig. 7, except for the target materials. The 2014 aluminum is the harder of the two materials shown, hence the lower penetration. Additional data in the higher velocity region for these curves should prove most interesting. If in the hypervelocity region the physical properties, except for densities, of the projectile-target combination are unimportant during the entire penetration process, these curves should merge into one. However, if the strength properties of the targets are important (possibly in the latter stage of crater formation), these curves will not converge. Because these data are definitely not in the hypervelocity region (nonhemispherically shaped cavity, as indicated in Fig. 5), additional experimentation is in progress at higher impact velocities.

Volume-Energy Relations - Figure 9 is a plot of cavity volume as a function of impact energy. The data represented by the straight line were obtained using 2014 aluminum spheres. The triangular points represent the data obtained when a one-piece aluminum projectile-shear disc combination was used. After shear, the projectile is cylindrical and has an initial mass of approximately 1 g. The last point on the graph was obtained for a 1.27-g cylinder. The scatter in these data is thought to be primarily due to variations in projectile mass. Two effects which could produce mass changes are variations in projectile

shear-out and friction between the projectile and bore during acceleration. By assuming a constant energy-volume relationship, as indicated by the sphere data, the projectile which had the highest energy had an actual mass of only 0.7 g, indicating a mass loss of 45 percent.

Figures 10 and 11 are graphs of the volume-energy relationship for several projectile-target combinations. All projectiles were saboted spheres. Based on the data shown, which are somewhat sparse, each curve with the exception of WC-Pb is either linear and intersects the origin or becomes linear as the impact energy is increased. Figure 12 is a plot of the impact energy E per unit of crater volume V as a function of striking velocity. For the Al-1100 F Al and WC-Cu curves, the ratios of E/V are constant at 690 joules/cm^3 and 1100 joules/cm^3 respectively. For the remaining curves in Figs. 10 and 11, the volume-energy relations are nonlinear in the low-impact-energy regions. However, if one considers only the linear portions of these curves, from approximately 4000 joules (100 joules for Al-Pb, Fig. 11), the form of the equation is

$$\frac{E}{V} = \frac{1}{M + c/E} \quad ,$$

where M is the slope and c is the extrapolated intercept value at $E = 0$. Dependent upon whether the intercept c is positive or negative, the ratio E/V either decreases or increases and asymptotically approaches the $1/M$ value for large energy values. Looking again at Fig. 12, the

solid curves indicate the region of experimental results; the dashed extensions are extrapolations which indicate the ultimate value of E/V when the impact is actually in the hypervelocity region. From a practical viewpoint, these ratios become constant. Since the WC-Pb curve, Fig. 10, is nonlinear, no extrapolation of the data to obtain an ultimate value of E/V is feasible. For the velocity region shown, E/V increases from 126 joules/cm^3 to 200 joules/cm^3. It should be emphasized that the ultimate E/V values for WC into steel, 1100 F Al, 2014 Al, and for Al-Pb were obtained by extrapolation. As additional data are obtained, these figures may require considerable revision.

Discussion of Cratering

From the data presented, there appear to be three regions of thick-target cratering. These are the low-velocity-impact regions, where the projectile remains intact, the transition region, where the projectile undergoes major deformation or shattering, and the region of hypervelocity impact. These regions of cratering have been previously identified by several investigators. For easily deformed projectiles such as aluminum, the low-velocity and transition regions may lose their identity. The three principal features of cratering discussed pertain to the attainment of a characteristic cavity shape, the penetration depth into various targets by aluminum and tungsten carbide projectiles, and the relationship between crater volume and energy of the impacting material. If we assume that craters in the hypervelocity region are hemispherical,

as indicated in Figs. 4 and 6, and that the volume-vs-energy relationships are linear in this region, Figs. 10 and 11 (excluding WC-Pb), we obtain the following penetration expression,

$$P = \left(\frac{3}{4 \pi K} \right)^{1/3} m^{1/3} v^{2/3} ,$$

where K is the energy/unit volume for a given projectile-target combination from Fig. 12, m is the projectile mass, and v is the impact velocity. A tabulation of calculated and actual penetrations is given in the following table.

Projectile-Target	K joules/cm^3	Velocity km/sec	Penetration (Measured) cm	Penetration (Calculated) cm
Al-1100 F Al	690	5	2.38	2.22
Al-1100 F Al	690	10	- - -	3.52
WC-Cu	1100	3	0.95	0.79
WC-Cu	1100	10	- - -	1.76
WC-Pb	200	2.6	2.86	2.53

It can be seen from this table and Fig. 4 that the more nearly the cavity is hemispherical, the closer is the agreement between measured and calculated penetrations. The above expression is strictly an empirical one which can be used to calculate the approximate depth of penetration as a function of impact velocity if the impact occurs in the hypervelocity region.

Spaced-Structure Damage

A study of the penetration of thin, spaced targets was recently initiated at NRL. Although the concept of spaced armor as a device for decreasing the penetration of low-velocity projectiles is well known, little research has been done relative to a spaced structure and hypervelocity fragment impact. Figures 13 and 14 are included in this paper to illustrate the effectiveness of a spaced target structure as compared with a single thick plate. Figure 13 shows the damage to three 1/16-in.-thick 24ST3 aluminum plates, 6 in. square, having a 4-in. separation between each pair of plates. The projectile was a 1-g aluminum cylinder having a velocity before impact of 5.34 km/sec. Although the third plate was damaged by bending, it sustained no perforation. Figure 14 is a front view of a 1-in.-thick 24ST4 aluminum target perforated by a 1-g aluminum cylinder having the same pre-impact velocity. In addition to target perforation, a large piece of aluminum was spalled from the rear surface. The scarred area above the hole and the small craters in the target are due to the gas-gun piston extrusion and small fragments from the piston and shear disc.

REFERENCES

1. Clark, A.B.J., and Boltz, P.T., "Vulnerability Mechanics," Report of NRL Progress, pp. 30-31, July 1956

2. Bailey, S.O., Clark, A.B.J., Hall, D.A., and Swift, H.F., "Facilities and Instrumentation at the NRL Hypervelocity Laboratory," NRL Report 5271, Feb. 1959

3. Halperson, S.M., and Fuller, R., "NRL Three Stage Light-Gas Gun," Report of NRL Progress, pp. 31-32, June 1960

4. Halperson, S.M., and Porter, C.D., "Interior Ballistics of the NRL Light-Gas Gun," NRL Memo. Rept. 1055, June 1960

LIST OF FIGURES

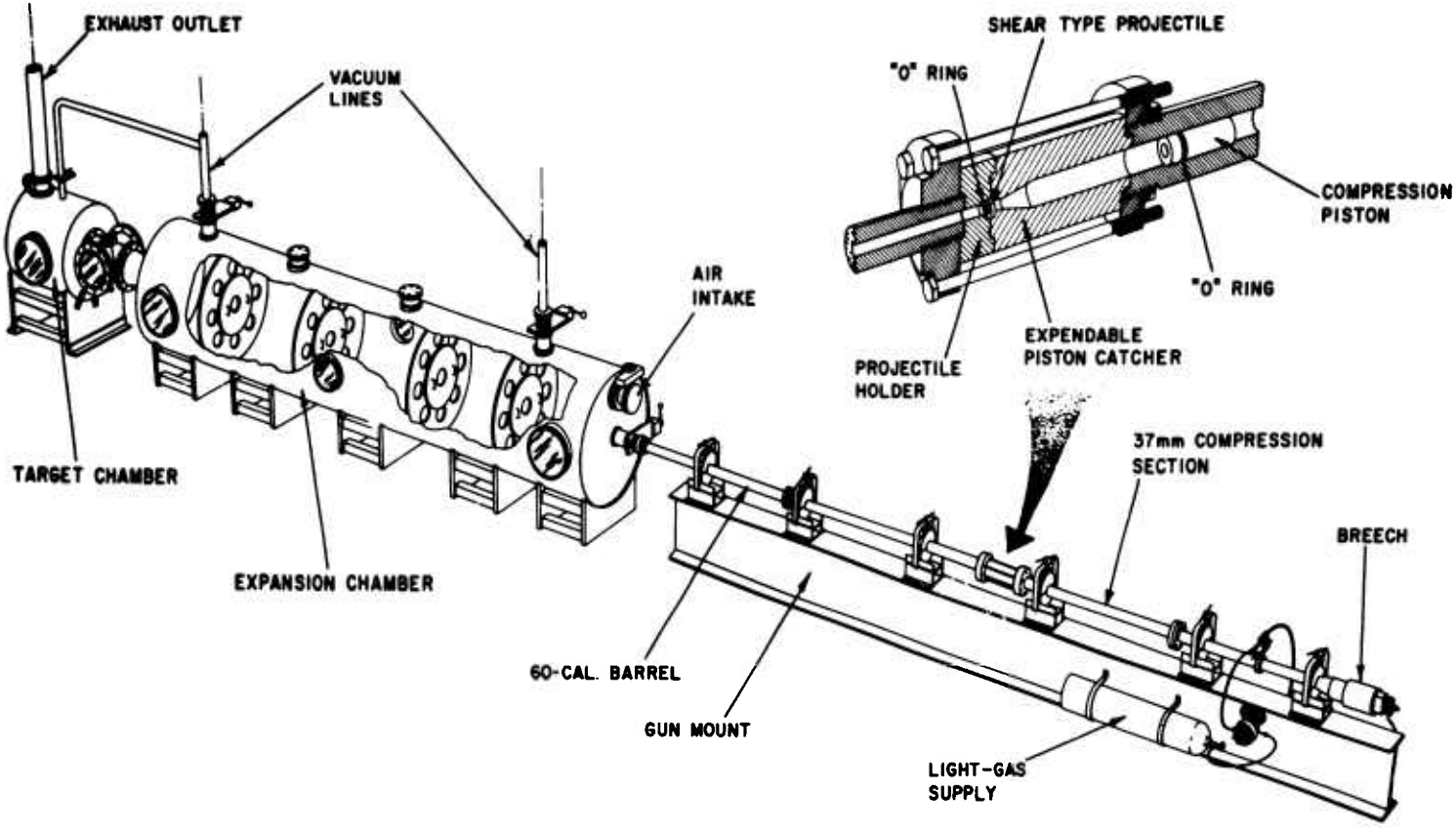

Fig. 1 - NRL hypervelocity ballistic range

Fig. 10: Crater Volume vs Impact Energy for Several Projectile-Target Systems

Fig. 11: Volume-Energy Curves for Al into Pb and WC into Cu

Fig. 12: Impact Energy/Crater Volume as a Function of Impact Velocity (The dashed curves indicate an extrapolation of the data. Ultimate E/V values for these curves are also shown.)

Fig. 13: Illustration of Reduction in Penetration Due to Projectile Shatter and Use of Thin Target Structure (Projectile vel = 5.35 km/sec)

Fig. 14: Photographs of 1-in.-thick 24ST4 Al Perforated by Al Projectile Having Same Mass and Velocity as Used in Fig. 13

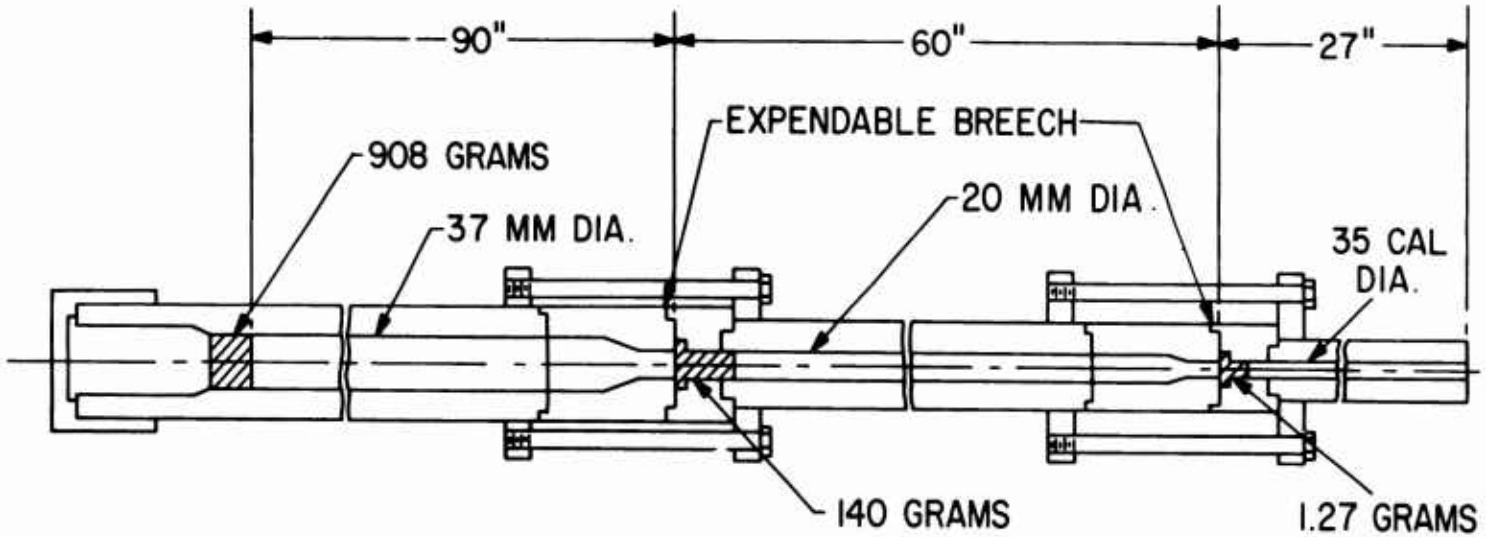

37 MM INITIAL GAS CONDITION: 700 PSI HELIUM
20 MM INITIAL GAS CONDITION: 400 PSI HELIUM
POWDER LOAD: 240 GRAMS OF 40 MM POWDER

Fig. 3 - NRL three-stage light-gas gun

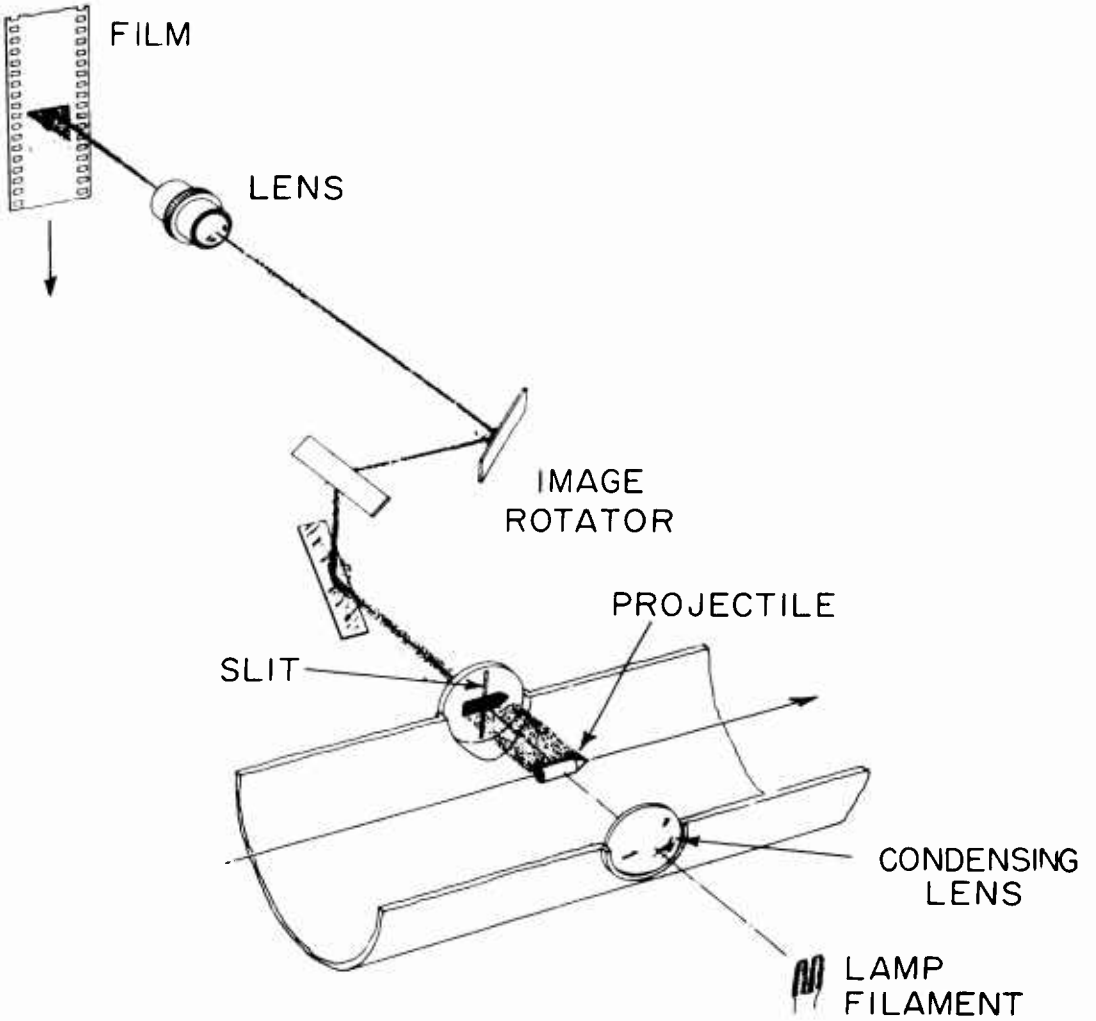

Fig. 2 - Diagram of single velocity-measuring station

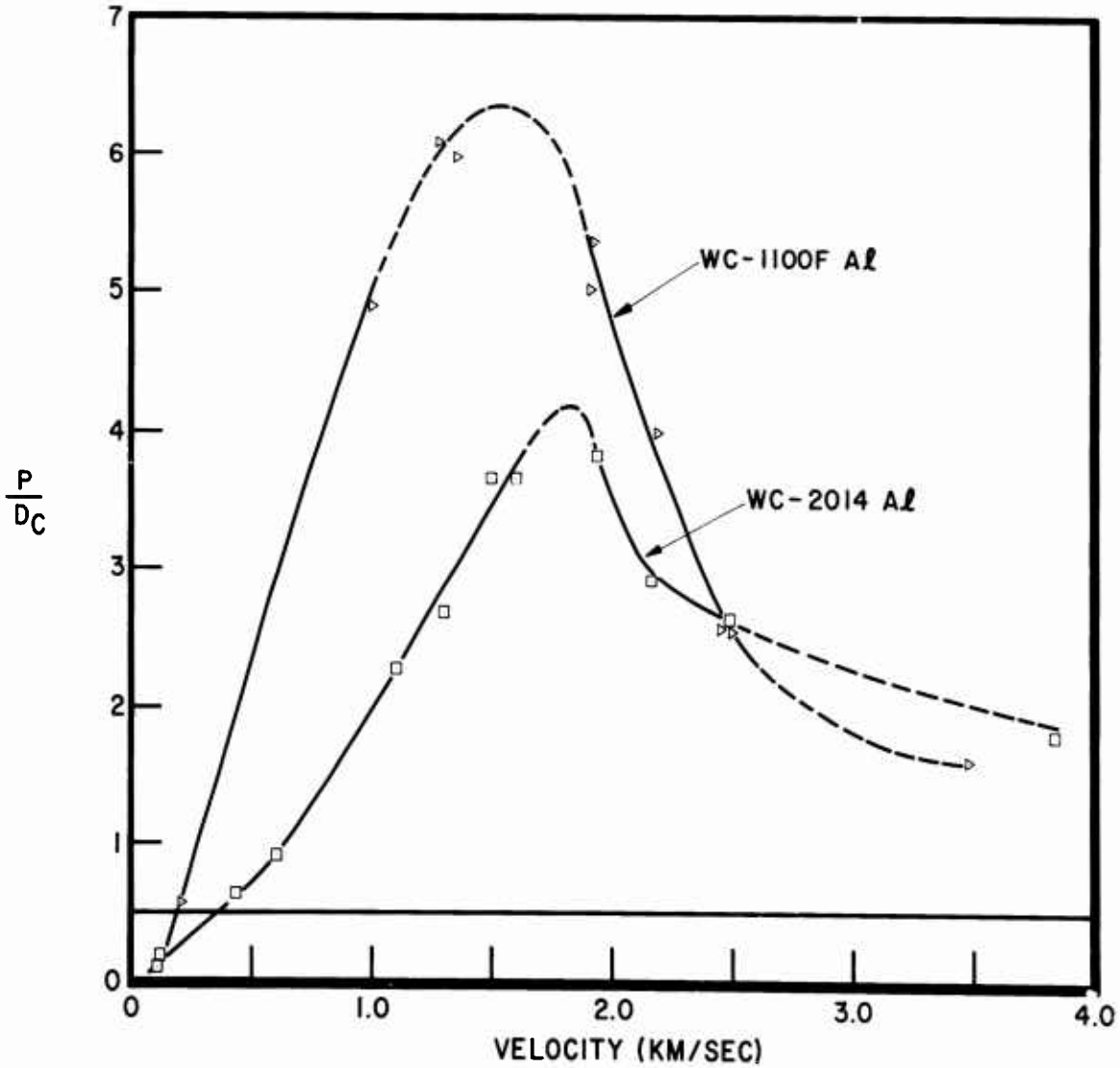

Fig. 5 - Crater shape as a function of impact velocity for tungsten carbide into two types of aluminum

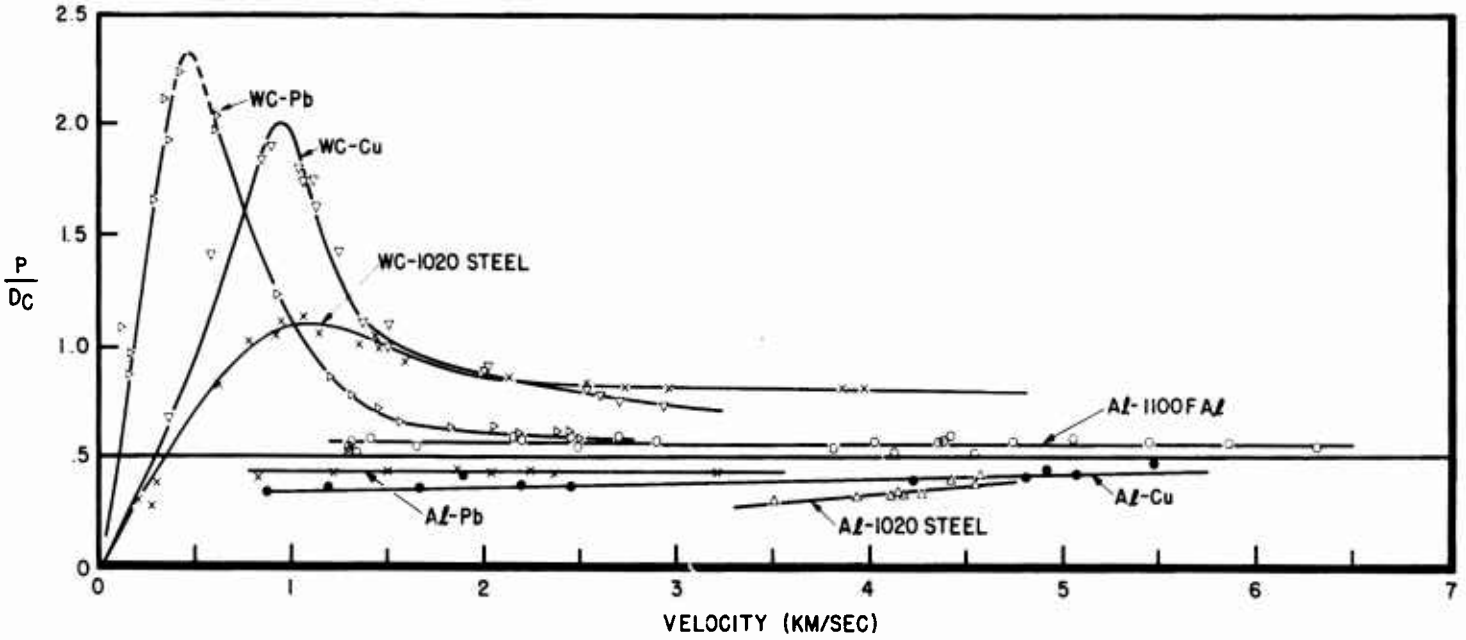

Fig. 4 - Graph of crater shape parameter vs impact velocity for several projectile-target systems

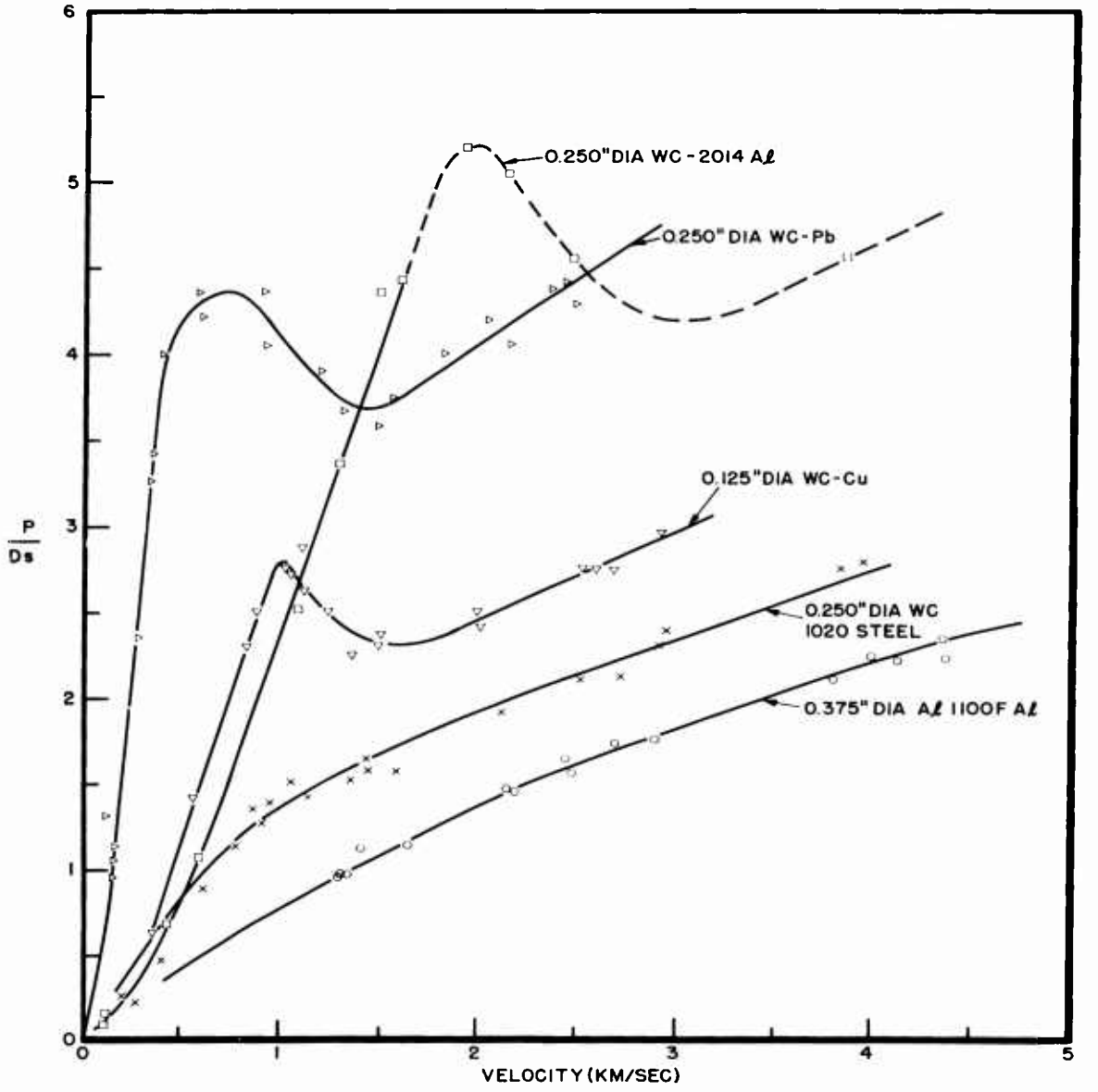

Fig 7 - Pentration into thick targets divided by projectile diameter as a function of impact velocity

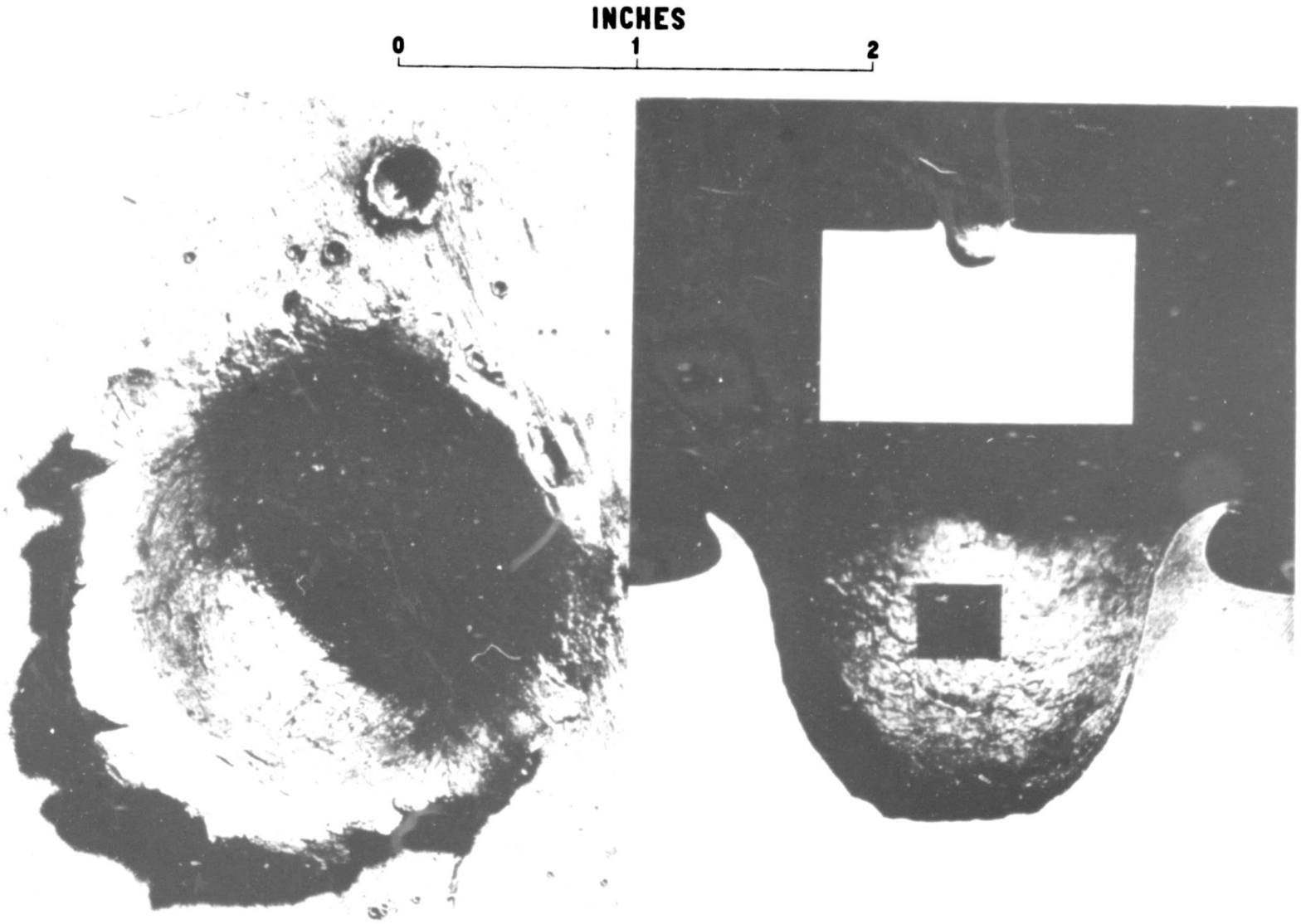

Fig. 6 - Front and sectional views of craters in 1100 F aluminum, impact velocity = 6.4 km/sec

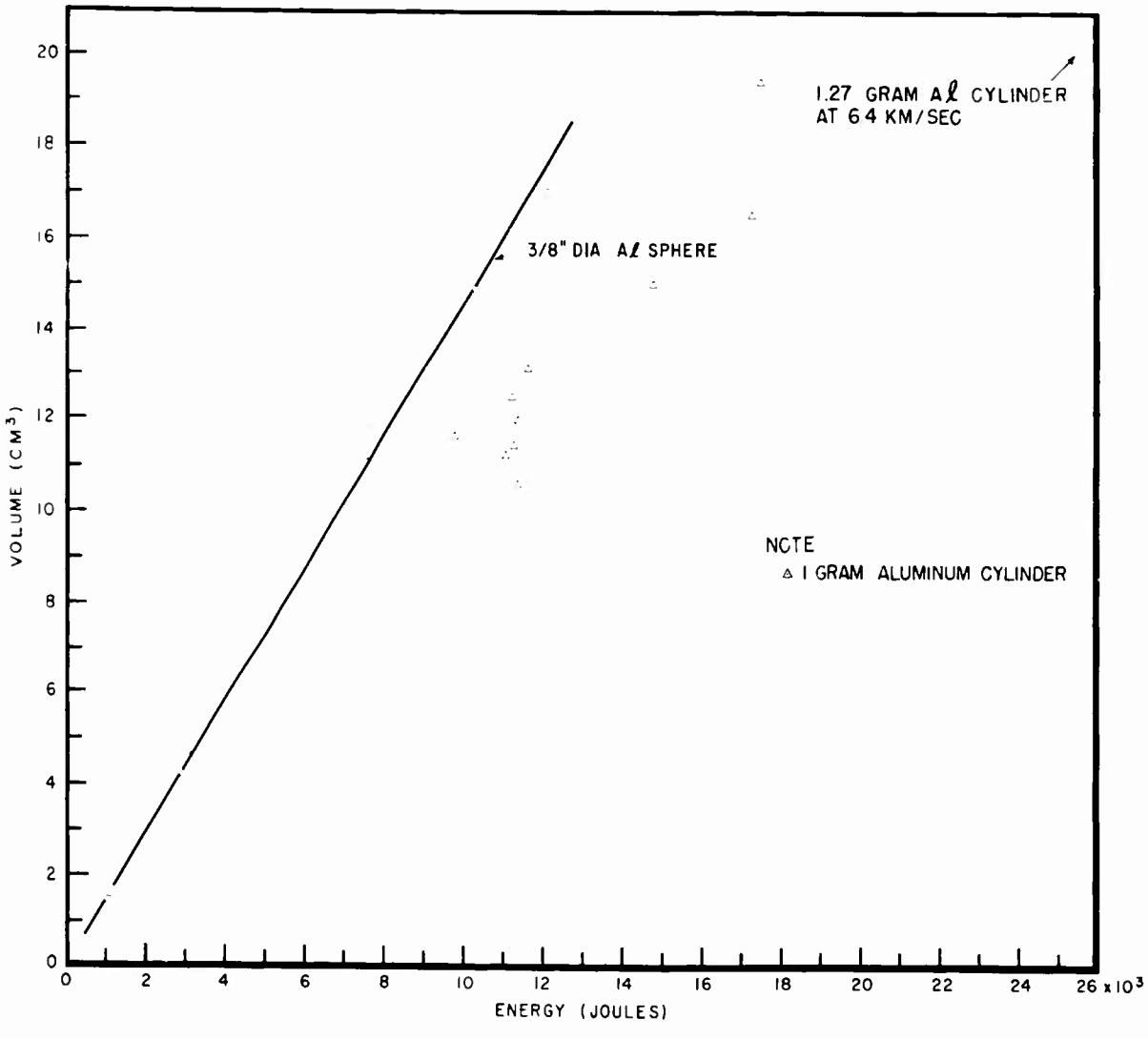

Fig. 9 - Crater volume vs impact energy for aluminum spheres and cylinders into 1100 F aluminum

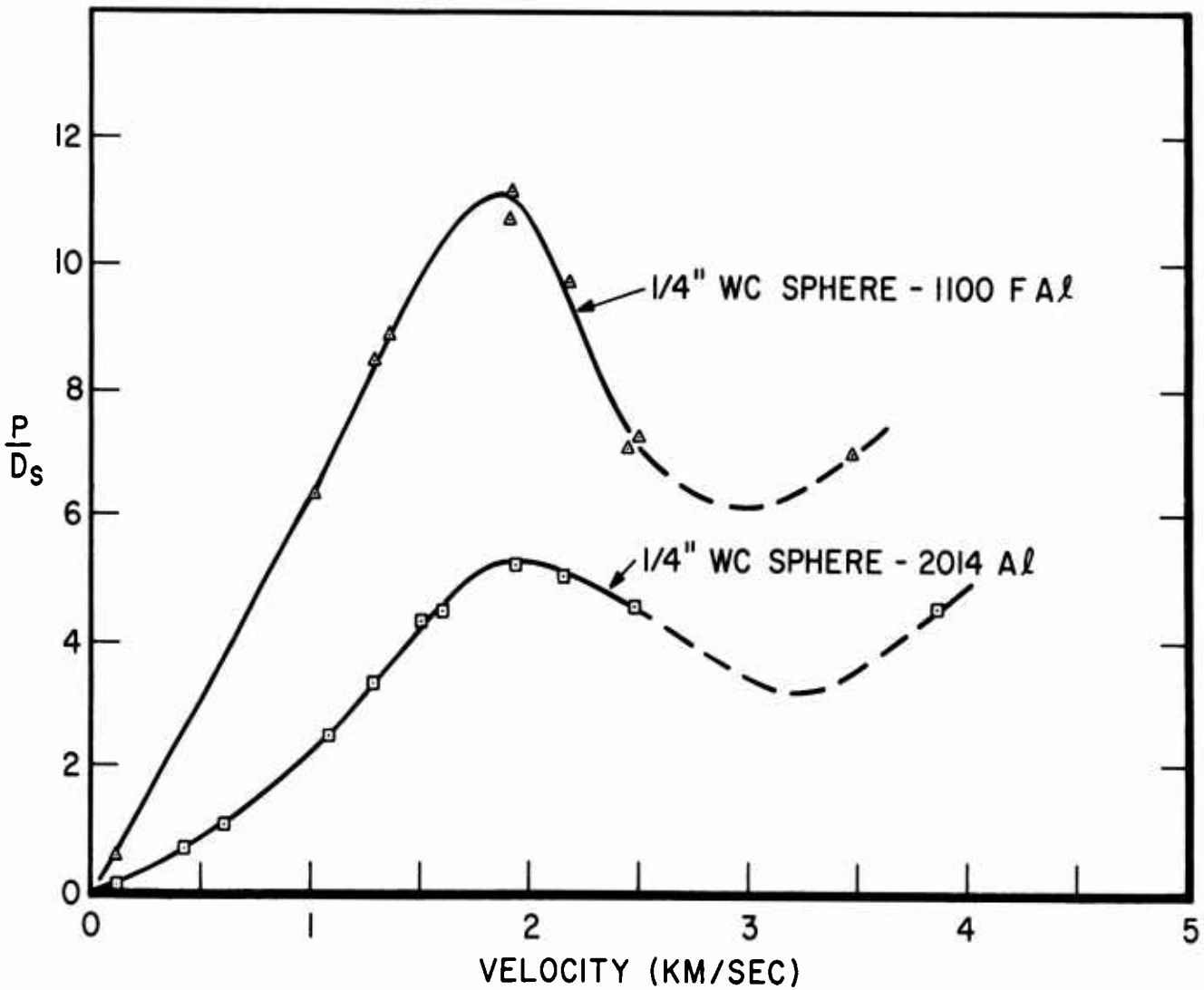

Fig. 8 - Ratio of crater depth/projectile diameter vs impact velocity for two types of aluminum

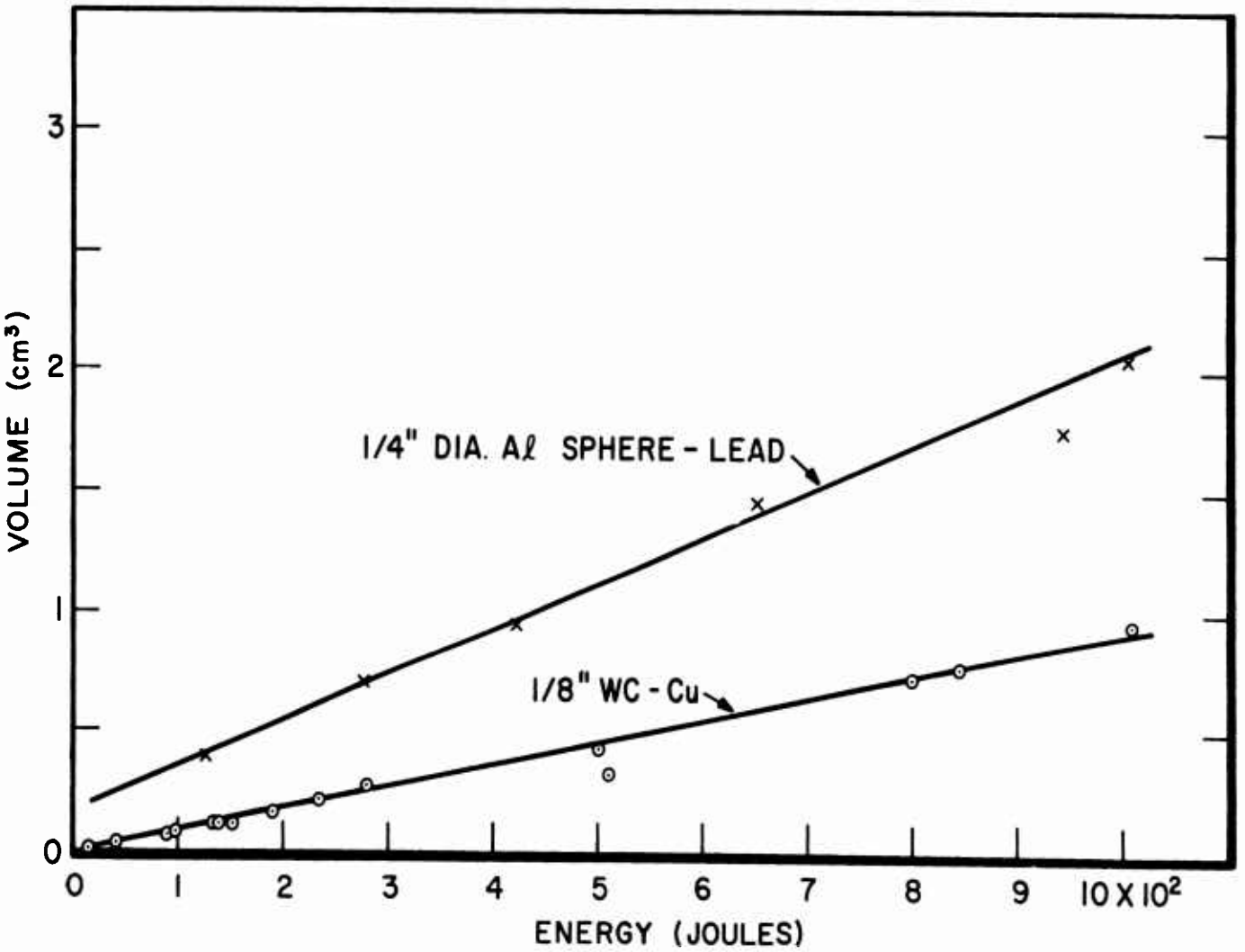

Fig. 11 - Volume-energy curves for Al into Pb and WC into Cu

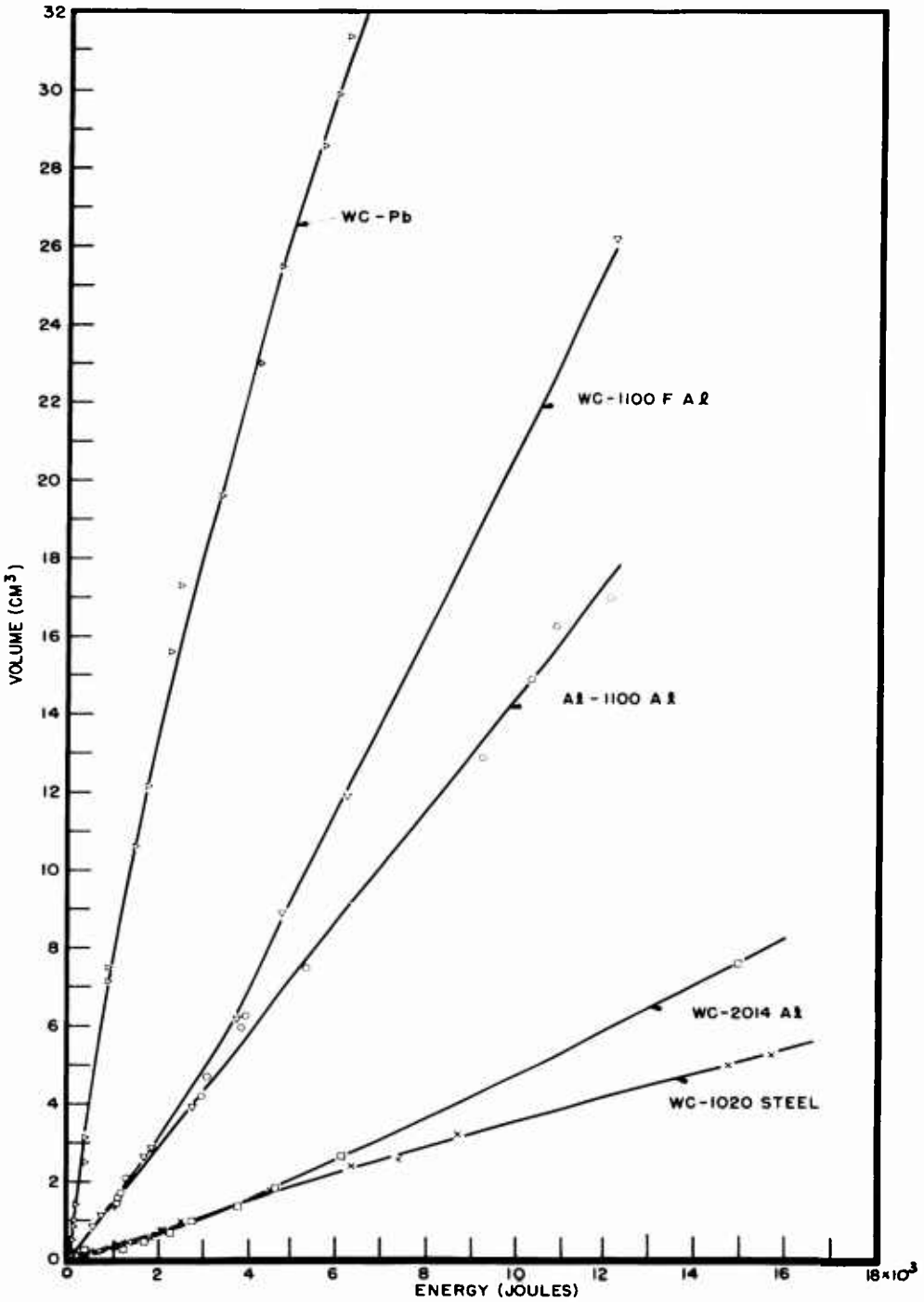

Fig. 10 - Crater volume vs impact energy for several projectile-target systems

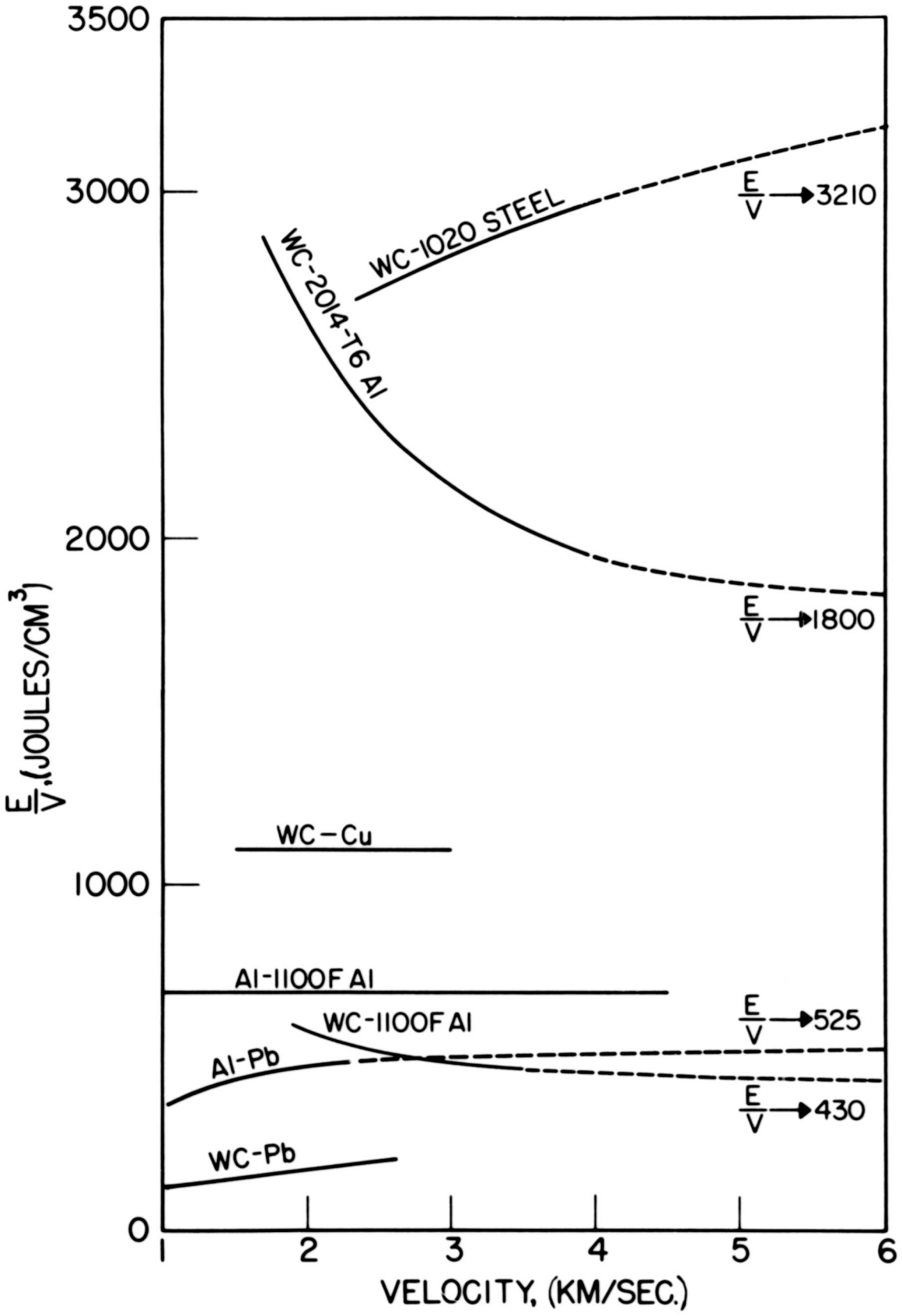

Fig. 12 - Impact energy/crater volume as a function of impact velocity. (The dashed curves indicate an extrapolation of the data. Ultimate E/V values for these curves are also shown.)

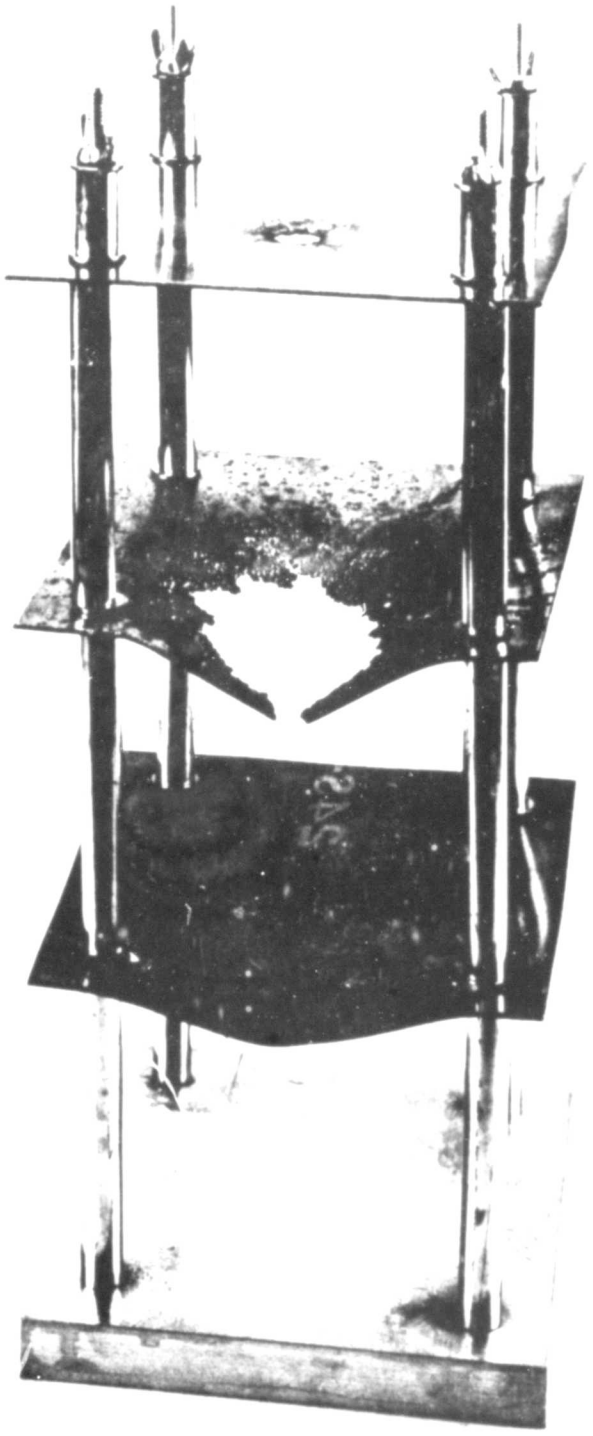

Fig. 13 - Illustration of reduction in penetration due to projectile shatter and use of thin target structure (projectile vel = 5.35 km/sec)

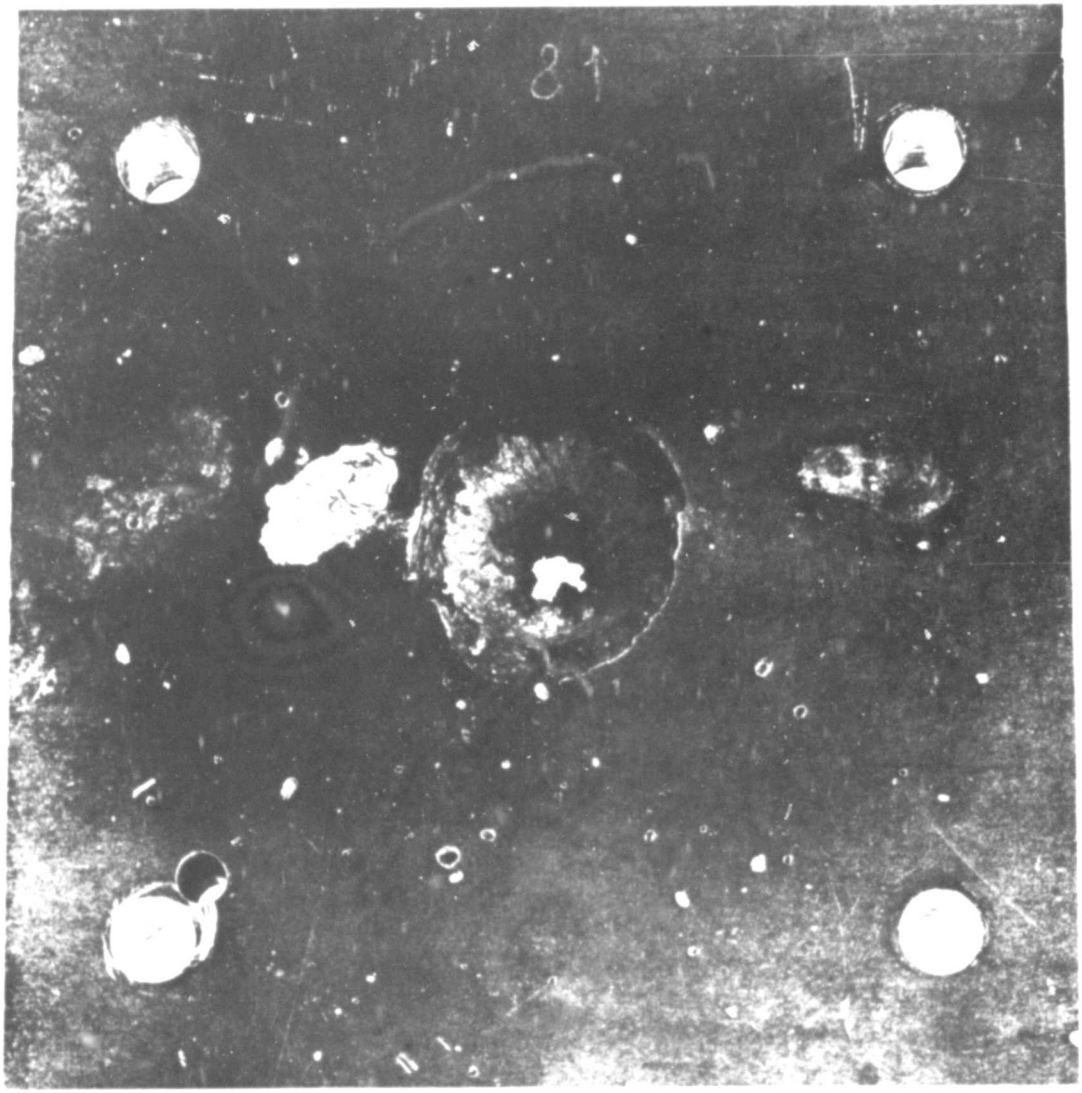

Fig. 14 - Photographs of 1-in.-thick 24ST4 Al perforated by Al projectile having same mass and velocity as used in Fig. 13